ELSEVIER

International Journal of Heat and Fluid Flow 21 (2000) 365–373

International Journal of HEAT AND FLUID FLOW

www.elsevier.com/locate/ijhff

Experimental investigation of turbulence modulation by solid particles in a grid-generated vertical flow

M. Hussainov [a,1], A. Kartushinsky [a], Ü. Rudi [a], I. Shcheglov [a], G. Kohnen [b], M. Sommerfeld [b,*]

[a] *Department of Aeromechanics, Estonian Energy Research Institute, Paldiski Mnt. 1, Tallinn 10137, Estonia*

[b] *Institut für Verfahrenstechnik, Fachbereich Ingenieurwissenschaften, Martin-Luther Universität Halle-Wittenberg, D-06099 Halle (Saale), Germany*

Received 22 June 1999; accepted 24 February 2000

Abstract

Experimental results dealing with the modulation of grid-generated turbulence by coarse glass particles in a vertical downward channel flow are presented. Glass beads with an average diameter of 700 μm and a mass loading up to 0.1 kg dust/kg air were brought into the flow by an individually designed particle feeder allowing to vary the initial velocity slip. In order to determine the gas flow characteristics, TiO_2 particles with an average size of about 2 μm were used as tracers. Two mono-plane grids with a mesh size of 4.8 and 10 mm generated an isotropic turbulence which decayed along the test section of 2 m length. The mesh Reynolds numbers for these grids, based on a mean air velocity of $U = 9.5$ m/s, were $Re_M = 3045$ and $Re_M = 6340$, respectively. Distributions of the mean velocity, the turbulence intensity along the channel axis and in different cross-sections obtained by Laser Doppler Anemometer (LDA) are presented. A degradation of signals from the glass particles due to coating of their surfaces by TiO_2 particles was observed during the measurements. The decay curves of the turbulence intensity in the streamwise direction showed an attenuation of turbulence intensity of the flow induced by the particles for both grids, while the presence of particles decreased the energy spectra at high frequencies.

Keywords: Grid-generated turbulence; Gas–solids flow; Glass beads; Turbulence modulation; Dissipation rate; Energy spectra

Notation

$A_\sim$	Doppler component of signal
$A_=$	constant component of signal
C	slope of the linear decay law for the decay curves
C_0	slope of the linear decay law for the unladen flow
C_s	slope of the linear decay law for the laden flow
c_μ	numerical constant in k–ε model of turbulence
D	flow dimension
d	diameter of the grid rod
E	spectral energy density
E_u, E_v	energy of the axial and transversal velocity fluctuations
$F1, F2, F3$	focal lengths of the lenses
f	spectrum frequency
k	turbulent energy
$\mathbf{k}$	wave number
L_E	integral length scale of flow
L_E^{SL}	integral length scale of the flow in terms of Snyder and Lumley notations
M	grid mesh size
$\mathbf{m}$	modulation depth of Doppler signal
$\mathbf{m}_p$	threshold value of counter
Re	Reynolds number of flow
Re_M	grid Reynolds number
Re_p	particle Reynolds number
S	area of test section
S_h	area of test section covered by grid
St_E	Stokes number, calculated by integral time scale of turbulence
St_K	Stokes number, calculated by Kolmogorov time scale of turbulence
T	time scale of flow
T_E	Eulerian integral time scale
t_K	Kolmogorov time scale
U	mean velocity of flow in streamwise direction
U_m	mean velocity of flow along the axis
U_s	mean velocity of particles in streamwise direction

* Corresponding author. Tel.: +49-3461-462879; fax: +49-3461-462878.

E-mail addresses: aeromeh@online.ee (M. Hussainov), martin.sommerfeld@vt.uni-halle.de (M. Sommerfeld).

[1] Tel.: +372-2-451442; fax: +372-6460206.

0142-727X/00/$ - see front matter
PII: S0142-727X(00)00022-9

u_i	instantaneous velocity of the flow in streamwise direction
u_i'	fluctuating velocity of flow
$\bar{u}$	mean velocity of flow
u_{rms}	root-mean-square velocity of the flow in streamwise direction
v_{term}	terminal velocity of particle
$2W_X$	diameter of probe volume in axial direction
X	co-ordinate directed along the axis of the channel
y	transversal co-ordinate
β	volume concentration of particles
δ	particle diameter
ε	dissipation rate of turbulence
η_{K}	Kolmogorov turbulence length scale
Λ	fringe spacing of probe volume
λ	inter-particle spacing
ν	kinematic viscosity of gas
ν_{t}	turbulent viscosity of gas
ν_0	turbulent viscosity of gas in the unladen flow
ν_{ts}	turbulent viscosity of gas in the laden flow
ρ	density of air
ρ_{p}	particle material density
σ	standard deviation
τ_{p}	particle time constant
æ	mass loading of flow

1. Introduction

The interaction of solid particles or liquid droplets with a turbulent gas flow is a prime issue in fundamental research. An overall understanding of the involved phenomena is important to improve the design of engineering devices employing gas flows in a vast number of industrial processes, e.g., the pneumatic conveying of solid materials, combustion of pulverized coal, spray drying, dispersion of pollutants, etc., which are found frequently in industry and nature.

The particular interest of the present experimental research is related to the modification of grid-generated turbulence by solid particles in a vertical downward channel flow. The mechanisms here are not very well understood in most situations due to a variety of parameters involved and it is very difficult to extract a reasonable amount of information from a single experiment. Moreover, the accuracy of the results obtained by experimental investigations has a tremendous impact on expected success of any model used to predict turbulence modification in a two-phase flow.

Two major reviews are available in the literature, where an attempt was made to classify turbulence modification in two-phase flows. In the study of Gore and Crowe (1989), the most relevant experimental investigations were analysed leading to a criterion for the modification of turbulence intensity depending on a scale ratio between the particle diameter and integral length scale of the flow, δ/L_{E}. Their analysis shows that particles attenuate turbulence, if the scale ratio is below 0.1 and they augment turbulence in case of a scale ratio beyond 0.1. In a later publication of Gore and Crowe (1991) different parameters were suggested, which may have an influence on the change of turbulence intensities, such as the density ratio ρ_{p}/ρ, the flow and particle Reynolds numbers, Re and Re_{p}, the scale ratio, δ/L_{E}, the relative turbulence intensity, and the volume fraction of particles β.

Hetsroni (1989) in his review argued that a criterion for determining turbulence attenuation/augmentation could be solely determined through the particle Reynolds number Re_{p}. He stated that for $Re_{\mathrm{p}} > 400$ wake effects become predominant leading to an enhanced turbulence production and hence to turbulence augmentation. Besides, different results were obtained for wall-bounded turbulent shear flows and free shear flows. Schreck and Kleis (1993) experimentally studied the mechanisms of the turbulence decay behind a grid with a mesh size of 17.8 mm, a mean velocity of 1 m/s, and for a flow loaded with either plastic or glass particles having an average size about 650 μm. Their experiments have shown that particles attenuated turbulence for various volume fractions within the range 0.4–1.5%. Comparing the results for the two-phase flow with the corresponding single-phase flow they found that the growth of energy took place at large wave numbers for the axial velocity component. For the transverse component the opposite has been observed, namely a reduction of the spectral density of energy at large wave numbers for both types of plastic and glass particles. The distribution of the total turbulent energy, namely $E = E_u + 2E_v$ (E_u and E_v are the energy of the axial and transverse velocity fluctuations, respectively), has shown a decrease of the spectral energy density E at large wave numbers. Kulick et al. (1994) studied a downward two-phase flow in a vertical channel. They used comparatively small copper particles with an averaged diameter of 70 μm and glass particles of 50 and 90 μm. For a mass loading up to 40% a reduction in the turbulence intensity was observed. Lance and Bataille (1991) investigated the influence of air bubbles on the turbulence intensity in a water flow behind a grid. They observed enhancement of turbulence caused by the bubbles. The distribution of the spectral energy density revealed a reduction in the small wave number range due to bubbles, whereas the large wave numbers were fed with the energy and took on higher values in comparison with the single-phase flow.

2. Experimental set-up

The experiments were carried out in a vertical two-phase wind-channel with a closed test section (Fig. 1(a)). The wind-channel consists of an intake (Pos. 1, Fig. 1(a)) with a diameter of 1 m, a contractor (Pos. 2, Fig. 1(a)) with the contour profiled by Vitoshinsky's formula according to Gorlin (1970) in order to smoothen the flow oscillations with the compression coefficient of 6.25, a transition duct (Pos. 3, Fig. 1(a)) (passage from round to square cross-section), a test section (Pos. 5, Fig. 1(a)) and a diffuser (Pos. 6, Fig. 1(a)). The test section was made of plexiglass and had a length of 2 m. The initial upper cross-section had dimensions of $200 \times 200\ \mathrm{mm}^2$ increasing gradually downstream up to $205 \times 205\ \mathrm{mm}^2$ at the flow exit. The geometry of the test section partially allowed us to compensate the boundary layer growth along the walls. Thus, the flow core could be kept uniform along the test section. There was a possibility to install optical glass windows along the full length of the test section in order to enable optical access for the Laser Doppler Anemometer (LDA) measurements. The downward air flow was created by a suction fan. The particles of the dispersed phase were brought into the flow by a special particle feeder (Pos. 8, Fig. 1(a)) installed in the intake of the wind-channel (Pos. 1, Fig. 1(a)). The glass particles were separated from the gas flow in the diffuser (Pos. 6, Fig. 1(a)) and then conveyed by pneumatic transport to a cyclone separator (Pos. 9, Fig. 1(a)). The reservoir for the glass particles (Pos. 8, Fig. 1(a)) was continuously refilled with those particles coming from the cyclone separator. The volume of the storage bin was 40 l. In this way 90 kg of the glass beads were available to perform the experiment in a continuous way for about 20 min,

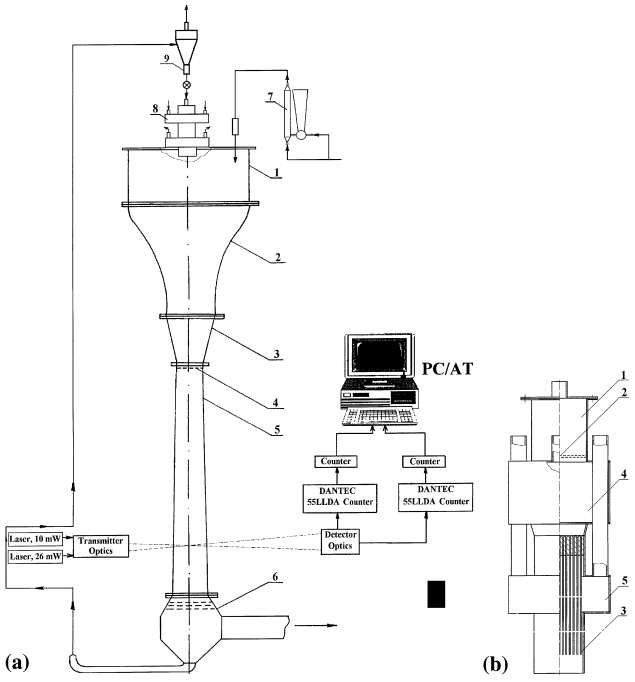

Fig. 1. Experimental set-up.

if the experiment was operated at a mass loading of 0.1 kg dust/kg air.

For injecting the dispersed phase particles into the channel inlet a special particle feeding system (Fig. 1(b)) was designed and manufactured which allows us to accelerate the glass beads up to a desired velocity in a bundle of thin tubes before they were introduced into the flow. The glass beads were brought from the reservoir (Pos. 1, Fig. 1(b)) into the tubes (Pos. 3, Fig. 1(b)) through dispersing grids (Pos. 2, Fig. 1(b)). In total 50 tubes were used which had a diameter of 4 mm and a length of 400 mm. Particles were accelerated in these tubes by an additional air stream. At the exit of the tubes, the air was separated by a suction fan through a chamber (Pos. 5, Fig. 1(b)). Thus, the particles were released into the inlet chamber at a given velocity.

TiO_2 particles with a particle size in the range 0.5–2 μm were used as tracers to measure the air velocities. The size distribution of the TiO_2 particles was analysed by a refractometer. The tracers from the seeding generator (Pos. 7, Fig. 1(a)) were brought into the flow throughout the intake (Pos. 1, Fig. 1(a)). The operation of the seeding generator was based on the principle of a fluidised bed. By means of a screw feeder the tracers were transported into the fluidised bed. Glass beads with an averaged diameter of 0.7 mm were also put into the fluidised bed and served as grinding material in order to break-up large aggregates of TiO_2 particles.

A turbulence generating grid was installed at the beginning of the test section (Pos. 5, Fig. 1(a)). Two types of mono-plane grids with square meshes were used in the experiments (Table 1).

Table 1

Grid	Mesh size M (mm)	M/d	Solidity S_h/S
1	4.8	2.53	0.487
2	10	2.5	0.49

3. Optical scheme and measurements

An LDA operated in a forward-scattering arrangement was used in order to measure the instantaneous velocities of the gas and particles. The LDA consisted of two channels for measuring gas and particle phase velocities simultaneously, i.e. the glass beads with a mass mean particle diameter of about 700 μm and TiO_2 tracers with a diameter in the range between 0.8 and 2 μm. This required the use of two lasers with a power of 26 and 10 mW, respectively, where the laser with the higher power was used for the tracer particles. The transmitting unit of the LDA channels formed two probe volumes with different dimensions in order to distinguish the velocities of the two groups of solid particles. The two probe volumes are placed above each other in vertical direction (about 2 mm between the centres of the volumes). The volume for coarse particles is situated above the volume for fine particles. Besides, the laser light for the two transmitting units have different polarisation.

One channel of the receiving unit was tuned for the registration of signals from the TiO_2 tracers. The second channel was adjusted to process signals from the dispersed phase glass beads. Each of the receiving channels was equipped with a separated optics, fibre cable, and photomultiplier (PM). Both channels were built in a modular way, and hence, it was possible to easily get access to the system and adjust the optical set-up according to the experimental requirements.

The dependence of the Doppler signals on the particles properties and the parameters of the LDA system was used for tuning both channels of the LDA in order to allow a reliable detection and separation of the Doppler signals from tracer and dispersed phase particles. The two receiving channels were designed to yield different signal amplitudes and frequencies for the tracer and glass beads, respectively. Hence, an amplitude, visibility, and frequency discrimination procedure allowed for a reliable separation of the signals from tracer and glass beads (Durst, 1982, 1983), so that any cross-talk between the phases was excluded by applying a combination of optical and electronic selection.

3.1. Channel for tracer measurements

The dimensions of the probe volume for measuring the gas velocity (i.e. the tracer) were determined by the flow conditions of the experiment. In order to prevent losses in the data rate resulting from an incomplete modulation of signals, a fringe spacing of $\Lambda = 5.43$ μm was selected according to the size of tracers ($\delta = 2$ μm). Thus, the Doppler frequencies for the trace signals were in a range 1.8–2.7 MHz, corresponding to a velocity in the range of 10–15 m/s. The tuning of the measurement channel for the tracer particles was performed by placing a rotating disc with a small aperture near the outer edge (i.e. 2–5 μm diameter) in the probe volume for the tracers. The diffracted light was collected by the receiver in the direction of small receiving angles. According to Van de Hulst (1957) and Kartushinsky et al. (1987), the scattered light from fine particles in the direction of small receiving angles is dominated by diffraction and hence is independent from the physical properties of particles (e.g., the refractive index). Therefore, the calibrating device simulated the real situation with the tracer particles rather closely. The selection of the signals from fine particles, smaller than 2 μm, was carried out automatically both by amplitude discrimination, where saturated signals were rejected, and by the modulation depth (i.e when $\mathbf{m} > \mathbf{m}_p$) with the help of a counter. The modulation depth $\mathbf{m}$ is defined as $\mathbf{m} = A_{\sim}/A_{=}$. Here $\mathbf{m}_p$ is the threshold value of the counter, $A_{\sim}$ represents the Doppler component of

the signal, and $A_=$ is the pedestal component of the signal. For excluding the cross-talk with the dispersed phase particles a special pedestal amplitude discriminator was used in the channel for the tracer (Frishman et al., 1987). This enabled to identify and seperate the Doppler signals from those large particles which passed through the edges of the small measurement volume and hence generated signals which were indistinguishable in amplitude from the signals emitted by fine particles.

3.2. Channel for the dispersed phase

In order to allow the detection of quite large particles also the size of the measurement volume needs to be rather large. Hence, the transmitting optics was designed to give a probe volume diameter of 1651 μm. This results in a fringe spacing of $\Lambda = 49.30$ μm. The optics consists of a diffractional beam splitter and lenses with focal lengths of $F1 = 360$ mm, $F2 = 110$ mm, and $F3 = 300$ mm, respectively.

The optics of the receiver and the sensitivity of the electronics were selected on the basis of preliminary investigations in order to get Doppler signals with a reasonable modulation and data rate. For the present experiments the resulting poor spatial resolution was not problematic. In the preliminary experimental investigations the voltage of PM was varied until a linear relationship between the amplitude of the Doppler signal and size of the glass beads in the diameter range 650–750 μm was obtained. Then the system was trimmed in order to get the maximum modulation in the Doppler signal. Hence, the cross-talk from tracer particles could be excluded by a proper choice of the sensitivity of the receiving module for the large particles.

A digital real time oscilloscope TDS 350/200 MHz was used for on-line control of the Doppler signals and the optimisation and tuning of the electronics. Besides, the oscilloscope digitised the Doppler signals for subsequent processing. The selected optical set-up of the channel for the large particles results in Doppler frequencies in the interval 0.2–0.3 MHz, corresponding to particle velocities about 10–15 m/s. In conclusion, besides the amplitude and visibility discrimination the signals of tracers and dispersed phase particles could be effectively separated by an additional frequency discrimination due to the use of two different optical systems. The frequency discrimination was realised by appropriate settings of the two band-pass filters.

The experiments carried out for the single-phase flow have shown a continuous registration of Doppler signals from the tracers in the respective channel. In the two-phase experiments, when 700 μm glass particles were brought into the flow, it was realised that after some time the micron tracers have covered the surface of the glass particles modifying their optical properties. This was the result of the recycling of the glass beads in order to allow continuous measurements. This effect implies, that we dealt with a situation, where the scattering properties of the glass particles have been modified during the experiments leading to a degradation of the Doppler signals. A continuous registration of the signals in the channel of the dispersed phase was found only in the case of clean glass particles. The situation slightly improved after decreasing the fringe spacing of the interference field to 24.83 μm and, correspondingly, increasing the total number of fringes in the probe volume to 66. Therefore, the experiments for the determination of the slip velocity between the two phases were performed by using clean (unused) glass beads. Figs. 2(a) and (b) depict the degradation of the Doppler signals received from the glass beads of 700 μm for a fringe spacing of 24.83 μm.

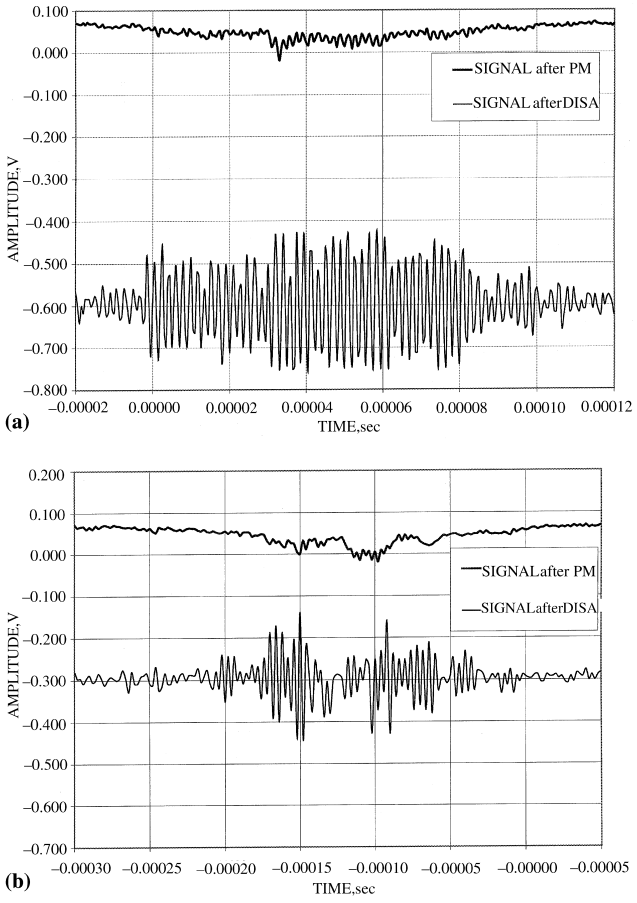

Fig. 2. (a) Signals after PM and DISA band-pass filter at the beginning of the experiment. (b) Signals after PM and DISA band-pass filter at the end of the experiment.

4. Data processing

The power spectra of the fluctuation velocities of the continuous phase were obtained at various distances from the grid in the centre of each cross-section. For the calculation of the power spectra 15 series of instantaneous velocity measurements were carried out at each location in order to obtain the required sample size. Each series of measurements included 2000 samples of the axial component of the instantaneous velocity. These series were registered only, if the registration times were less or equal to 0.4 s. The registration time depended on the concentration of tracers taking on values in the range 0.2–0.4 s with an average value of 0.3 s. Thus, the initial assembly of samples of the instantaneous velocities included 30 000 samples with an average time interval between each single sample of 150 μs, which led to an average sample frequency of 6.6 kHz.

Each series of the instantaneous velocities was processed by an amplitude and temporal filtering procedure. An example of a typical registered sequence of the velocity fluctuations of the gaseous phase is presented in Fig. 3. It is obvious, that certain samples are out of the expected fluctuation range (indicated with A). The reason for such large values is related to the increase of the level of background noise in the LDA channel of the gaseous phase. The number of such out-of-range values was less than 0.2% of the total number of samples for the gas velocity and it did not depend on the presence of the dispersed phase particles in the flow. The initial data sequence of the

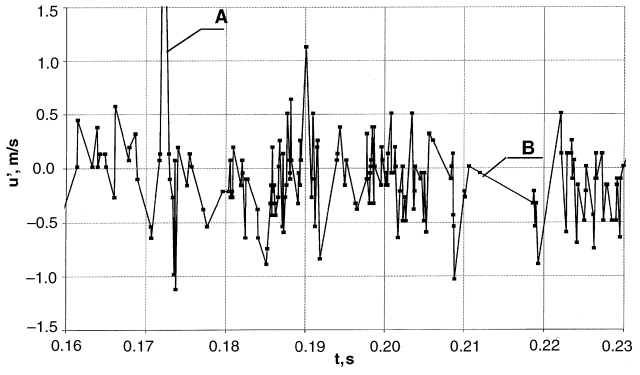

Fig. 3. Initial sequence of the instantaneous velocity.

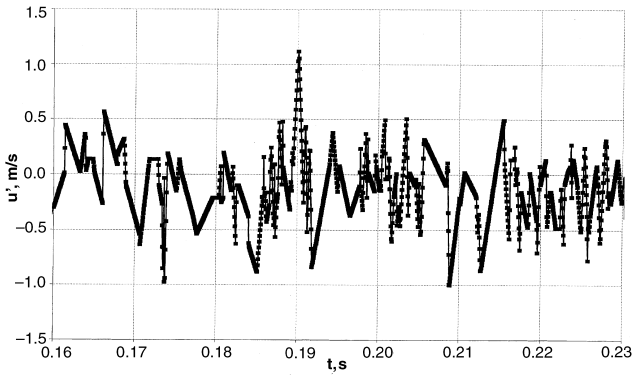

Fig. 4. Initial sequence of the instantaneous velocity after filtering and discretisation.

instantaneous gas velocity also contain large time intervals between successive samples (indicated with B) which were substantially larger than the turbulence integral time scale and were caused by non-uniform seeding of the flow. The number of such time intervals usually did not exceed 0.4% of the total number of samples.

The amplitude filtering was based on the 3σ-rule (Kulick et al., 1993), which is typical for a Gaussian distribution (here σ is the standard deviation). According to this rule, beyond the limits of the $\pm 3\sigma$ there are at most 0.27% of all values of the samples. Applying the 3σ-technique was started with the calculation of the standard deviation according to the formula

$$\sigma = \sqrt{\frac{1}{N-1}\sum_{i=1}^{N}(u_i - \overline{u})^2}$$

with the mean velocity obtained from

$$\overline{u} = \frac{N}{\sum_{i=1}^{N}\frac{1}{u_i}}.$$

Secondly, the value of an instantaneous velocity was determined from the initial sequence of data, for which the fluctuating velocity component was beyond the 3σ range. Then this value was replaced by the average value for the nearest neighbouring samples. Next, σ was calculated again and the whole procedure was repeated until all values from the data sequence satisfied the condition $|u_i'| \leqslant 3\sigma$. The temporal filtering was based on the determination of the time intervals between two successive samples exceeding 0.005 s. In such a case, the data have been shifted along the time axis by this value.

A linear time discretisation with a constant time step of 50 μs was imposed on the filtered data. Figs. 3 and 4 depict an example of the initial sequence of data and a data sequence after filtering and discretisation. It is obvious that the amplitude filter effectively suppresses the noise samples **A**. The temporal filter cuts the interval **B** which occurred in the absence of tracers.

The analysis of the time series has shown that the presence of such out-of-range values (**A**) increases the turbulent energy at the high-frequency end, whereas the presence of large time interval (**B**) lead to an increase of the turbulence energy at the low-frequency end of the energy spectrum. Hence, the amplitude and temporal filtering allows us to obtain reliable energy spectra of the turbulence.

An estimation of the power spectra was carried out for a length of 2048 bins where 1024 bins were overlapping the ranges according to Walch's periodogram and with the help of a rectangular window of data (Marple, 1986). Thus, each series of samples allowed to calculate on average about six estimates of spectra. The length of the data sequence was 2048 bins which corresponds to a total time interval of 0.1 s. This was substantially larger than the time scale of the flow which was 0.02 s, hence, the data are statistically independent. The final spectra were obtained by averaging of 90 independent estimations of the real spectra.

The velocities of the glass particles were measured by the channel of the LDA system which was tuned for the dispersed phase with the parameters presented in Table 2. As mentioned above, high-quality signals could only be received from clean glass particles. Hence, for the evaluation of the slip velocity the experiments were conducted with clean glass beads only (i.e. without recycling the particles).

5. Experimental conditions

5.1. Mean velocity and average fluctuations

The basic series of experiments was carried out when the mean air velocity of the single-phase flow was about 9.5 m/s. In Fig. 5 profiles of the averaged streamwise velocities and their fluctuations just above the grid for the laden and the unladen flow are shown. It is evident, that the non-uniformity of the flow (standard deviation) for the averaged velocities is less than 0.5% and for the fluctuation values is less than 6% in the two-phase flow. According to the experimental results, the turbulence intensity of a single-phase flow is about 3.5% at the final stage of the turbulence decay. This is considerably larger than it was found in other experiments (Hinze, 1975) and probably caused by a high initial turbulence level of flow, which was generated above the grid due to the presence of the particle feeder in the intake (Pos. 1, Fig. 1(a)). Thus, the experiments were carried out under a slightly excessive turbulence level above the grid, which did not allow to compare the present results with those of other authors. Nevertheless, the measurements permit to draw conclusions about the particle influence on the turbulence structure of the carrier phase in a two-phase turbulent flow.

5.2. Particle velocity and mass loading

The particles were preliminary accelerated up to a certain velocity before entering the flow, i.e., the particles moved in the flow with a negative velocity slip (ahead of the flow). In the absence of the turbulence generating grid, the particle feeder (Pos. 8, Fig. 1) allowed to produce a large negative slip velocity, roughly equal to the terminal velocity of the particles (about 5 m/s). The measurements showed that the situation

Table 2
Parameters of the LDA system

	Channel of the tracer particles	Channel of the disperesed phase
Transmitting optics		
Wavelength of the laser	0.6328 μm	0.6328 μm
Focal length of the front lens	300 mm	300 mm
Beam separation	35.0 mm	3.85 mm
Diameter of the measuring volume	87.9 μm	1651 μm
Fringe spacing	5.43 μm	49.30 (24.83) μm
Fringe number	16	33 (66)
Receiving optics		
Off-axis angle	3.0°	5.8°
Focal length of the collimating lens	58 mm	58 mm
Distance from the measuring volume to the receiving optics	250 mm	422 mm

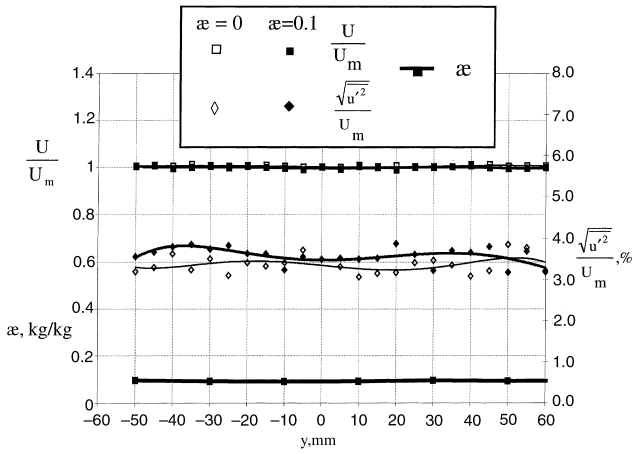

Fig. 5. Profiles of the averaged velocities, their fluctuations and the particle mass concentration in the initial cross-section. Unladen flow: light symbols, thin lines; laden flow: filled symbols, solid lines.

was different in the presence of the grid. There only 35% and 40% of particles for grid 1 and 2, respectively, had a mean streamwise velocity component exceeding the mean gas velocity. Only some particles (about 15%) moved with a slip velocity larger than 3 m/s. This behaviour may be explained by the following effects. One possible reason may be a saltating motion of the particles in the feeding system, i.e., particle–wall collisions in the injection tubes. So, the particle motion is characterised by a relatively strong transverse velocity component at the exit of this device (Pos. 8, Fig. 1). Another reason is likely connected with the influence of particle size distribution, which resulted in a scatter of the particle velocities due to their different inertia. Finally, some fraction of particles may collide with the grid rods and rebounded in various directions, so that the momentum originally contributed to the main flow direction is partly redistributed to the transverse direction. This effect became stronger with decreasing the grid mesh size.

The mass flow of the dispersed phase was measured with the help of an isokinetic sampling method (Laats and Frishman, 1970). The profile of the particle mass flow across the channel was measured simultaneously by sampling with 10 isokinetic tubes having an inner diameter of 2 mm. The sampled air passed through a rotameter, and the particles precipitated on the filter and then were weighed after a definite period of time. With the measured mass flow and the velocities of the gaseous and dispersed phases, the profiles of the particle mass concentration were calculated for every test series. The maximum mass loading of particles which could be established with the particle feeding device was about 0.12 kg dust/kg air. The non-uniformity of the particle mass concentration in a cross-section did not exceed 3.5% (Fig. 5).

6. Results and discussions

Measurements were performed in the following cross-sections downstream of the grid: $X = 63$, 95, 126, 251, 383, 503, 692, 1264 mm. The energy spectra for the streamwise velocity fluctuations of the gas phase have been determined at the axis of the channel for laden and unladen flow in the above mentioned cross-sections. Profiles of the streamwise velocity component of the gaseous and dispersed phases have been obtained in some cross-sections as well. The decay curves in Figs. 6 and 7 show the behaviour of the quantity $U^2/\overline{u'^2} = U^2/u^2_{\mathrm{rms}}$ along the channel axis downstream the grid 1 and 2, respectively, for laden and unladen flows. These results indicate, that the turbulence intensity of the flow decays up to the cross-section $X/M \sim 90$ for grid 1 and $X/M \sim 40$ for grid 2 and then remain almost constant further downstream. This corresponds approximately to initial turbulence levels of the flow without a turbulence-generating grid. From these figures one can also conclude that the glass particles with a

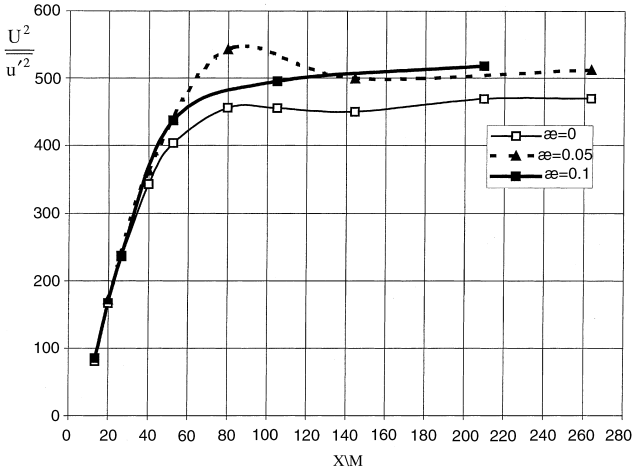

Fig. 6. Modification of the turbulence intensity behind the grid 1 ($M = 4.8$ mm).

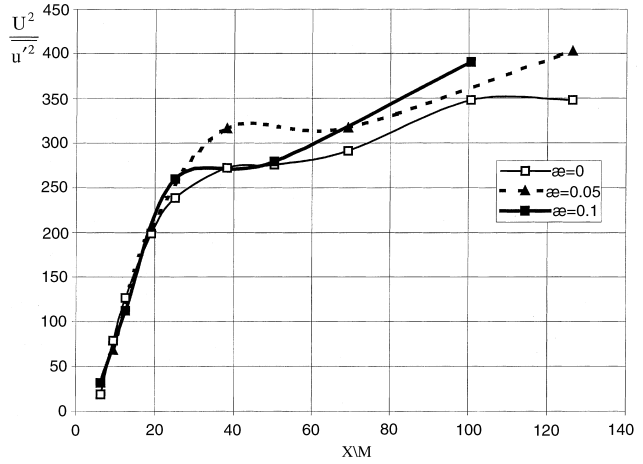

Fig. 7. Modification of the turbulence intensity behind the grid 2 ($M = 10$ mm).

mean diameter of 700 μm result in a decrease of the turbulence intensity. This decrease is more pronounced for grid 1 than for grid 2. The energy decay curves are adequately approximated by the following correlations

$$\frac{U^2}{u_{\mathrm{rms}}^2} = 8.19\left(\frac{X}{M} - 0.22\right) \quad \text{for single-phase flow (grid 1)}, \quad (1)$$

$$\frac{U^2}{u_{\mathrm{rms}}^2} = 8.92\left(\frac{X}{M} - 1.24\right) \quad \text{for two-phase flow (grid 1)}, \quad (2)$$

$$\frac{U^2}{u_{\mathrm{rms}}^2} = 11.42\left(\frac{X}{M} - 3.09\right) \quad \text{for single-phase flow (grid 2)}, \quad (3)$$

$$\frac{U^2}{u_{\mathrm{rms}}^2} = 12.55\left(\frac{X}{M} - 3.7\right) \quad \text{for two-phase flow (grid 2)}. \quad (4)$$

The initial energy spectrum of the streamwise velocity fluctuation of the gaseous phase was smoothed using an averaging procedure over an ensemble of the neighbouring values. For a given energy value one can calculate the smoothed values in the following way:

$$E'(f_i) = \frac{1}{9}\sum_{j=i-4}^{i+4} E(f_j), \quad i = \overline{5, N-4},$$

$$E'(f_i) = \frac{1}{2i-1}\sum_{j=1}^{2i-1} E(f_j), \quad i = 1, 2, 3, 4,$$

$$E'(f_i) = \frac{1}{2(N-i)+1}\sum_{j=2i-N}^{N} E(f_j), \quad i = \overline{N-3, N}.$$

Here $E(f_i)$ and $E'(f_i)$ are the initial and smoothed energy spectra, respectively. Such smoothing allows us to better identify the influence of particles on the energy spectra of the carrier flow as a whole, although the information about minor details of the spectrum vanishes, as one can see from Figs. 8 and 9.

In the high-frequency end of the spectrum (frequencies higher than 1 kHz) a decrease of the turbulence energy was observed for grid 1 in almost all considered cross-sections.

The turbulence structure of a single-phase flow behind the grid was conditioned by the whole set of flow parameters, such as the mean flow velocity U, the grid Reynolds number Re_M, the grid mesh size M, and the ratio between the mesh size and

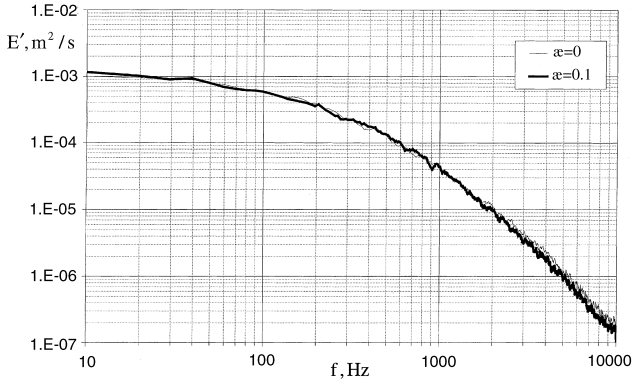

Fig. 8. The smoothed energy spectra for single- and two-phase flows in the cross-section $X = 126$ mm (grid 1).

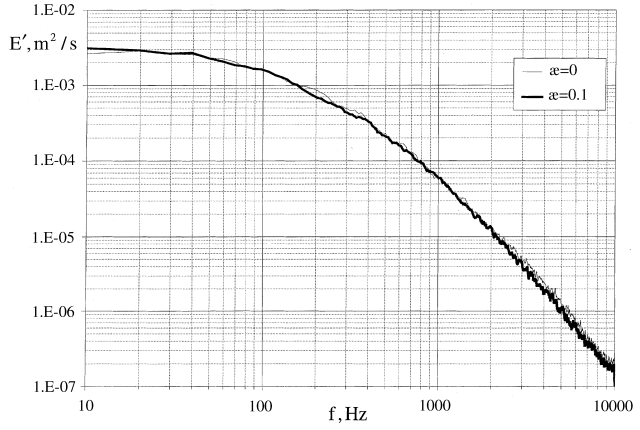

Fig. 9. The smoothed energy spectra for single- and two-phase flows in the cross-section $X = 126$ mm (grid 2).

the diameter of the grid rod, namely M/d (Hinze, 1975). Parameters of the single-phase flow and the relevant parameters related to the dispersed phase at the cross-section $X/M = 26$ are presented in Tables 3 and 4.

Here L_{E} and $L_{\mathrm{E}}^{\mathrm{SL}}$ are the integral length scales of the turbulence dissipation calculated as $L_{\mathrm{E}} = k^{3/2}/\varepsilon$ and in the particular case of the grid-generated turbulence according to Snyder and Lumley (1971) as $L_{\mathrm{E}}^{\mathrm{SL}} = UE(0)/4\overline{u'^2}$, where $E(0)$ is the spectral energy of the streamwise velocity component in vicinity of very low frequencies. Table 3 shows that the length scales calculated from the turbulent kinetic energy, its dissipation rate and the one determined according to Snyder and Lumley (1971) take on values of the same order of magnitude for both grids. The Kolmogorov length scale is calculated from:

$$\eta_{\mathrm{K}} = \left(\frac{\nu^3}{\varepsilon}\right)^{1/4}.$$

The turn-over times for the smallest and largest eddies (i.e., the Kolmogorov time scale and the integral time scale of turbulence) and the time of the aerodynamic process are calculated as $t_{\mathrm{K}} = \sqrt{\nu/\varepsilon}$, $T_{\mathrm{E}} = L_{\mathrm{E}}/U$, and $T = D/U_{\mathrm{m}}$, respectively.

The Stokes numbers, which are calculated both with the turn-over time of the smallest eddies and with the integral time scale of turbulence based on the particle response time τ_{p} can be expressed as follows: $St_{\mathrm{K}} = \tau_{\mathrm{p}}/t_{\mathrm{K}}$, $St_{\mathrm{E}} = \tau_{\mathrm{p}}/T_{\mathrm{E}}$, where

Table 3
Turbulence quantities for the single-phase flow at $X/M = 26$

M (mm)	4.8	10
ε (m^2/s^3)	49.22	21.46
L_E (m)	1.7×10^{-2}	2.6×10^{-2}
L_E^{SL} (m)	1.125×10^{-2}	1.956×10^{-2}
η_K (m)	0.91×10^{-4}	1.12×10^{-4}
t_K (s)	5.5×10^{-4}	8.36×10^{-4}
T_E (s)	1.78×10^{-3}	2.74×10^{-3}
T (s)	0.021	0.021

Table 4
Relevant parameters characterising the dispersed phase

M (mm)	4.8	10
δ (mm)	700	700
ρ_p (kg/m^3)	2500	2500
v_{term} (m/s)	5.761302	5.761302
œ (kg/kg)	0.1	0.1
β	3.1×10^{-5}	3.1×10^{-5}
$U - U_s$ (m/s)	1.5	2
Re_p	70	93
τ_p (s)	4.5	4.5
St_K	8.2×10^3	5.4×10^3
St_E	2.65×10^3	1.64×10^3
λ (m)	8.26×10^{-2}	8.26×10^{-2}
λ/δ	118	118
δ/η_K	7.7	6.25
δ/L_E^{SL}	6.22×10^{-2}	3.58×10^{-2}

$\tau_p = \rho_p \delta^2 / 18 \rho v$. In addition, according to Kenning and Crowe (1997), the ratio between the inter-space particle distance and the particle size can be written as

$$\frac{\lambda}{\delta} = \left(\frac{\pi}{6\beta}\right)^{1/3} - 1,$$

where the volume fraction β is given by $\beta = \rho æ U / \rho_p U_s$ and æ represents the integral mass loading.

According to Crowe et al. (1996) the glass beads used in the experiment can be considered as large particles, since the Stokes numbers for both trubulence time scales are much larger than unity, i.e. $St_E \gg 1$ and $St_K \gg 1$. Besides, the particle size exceeds the size of the smallest turbulent eddies about six times ($\delta/\eta_K \approx 7.7$ for grid 1 and $\delta/\eta_K \approx 6.3$ for grid 2). Since the flow is dilute, the motion of these particles should not produce a significant feedback effect on the flow. On the other hand, according to Gore and Crowe (1989), the influence of particles on the turbulence modulation of the carrier flow roughly depends on the parameter δ/L_E. In the present case $\delta/L_E \approx 0.04$ for grid 1 and $\delta/L_E \approx 0.03$ for grid 2. Thus, the particles should attenuate turbulence of the carrier flow which was observed in the experiments.

The map introduced by Elghobashi (1991) shows as well the influence of the inter-particle spacing normalised by the particle diameter on the turbulence modulation. In our notation this ratio is described by λ/δ and takes on a value of 118. This is close to the limit of $\lambda/\delta = 100$, where the two-way coupling regime is of considerable importance. Hence, we deal with a transition region, where one can expect to have some influence of the particles on the turbulence of the carrier flow. Based on the calculated values of St_K and St_E in connection with parameter of λ/δ we shift along the vertical axis of Elghobashi's map (1991) to the domain, where the influence of particles on the turbulence modulation would take place resulting in turbulence enhancement, which was not observed in the present experiment.

One result of the present investigation is the detection of an increase of the decay rate of the turbulence intensity in laden flow, which is accompanied by a reduction of the spectral energy in the high-frequency end. This result agrees with data by Schreck and Kleis (1993), who observed an increase in the energy dissipation rate and a reduction of the spectral energy in the same frequency sub-range.

To explain the correspondence between the two observed effects, an increase of the decay rate of the turbulence intensity and a reduction of the spectral energy in the high-frequency end, let us perform a comparison between the values of the turbulent viscosity of the carrier flow calculated for the two- and single-phase flows. This value is a function of the turbulent kinetic energy k and its dissipation rate ε and it is calculated as

$$v_t = c_\mu \frac{k^2}{\varepsilon}.$$

In the initial period of the turbulence decay we observe a linear dependence on the distances downstream of the grid

$$\frac{U^2}{\overline{u'^2}} = C\left(\frac{x}{M} - A\right).$$

Here M is the grid mesh size, A and C are the constants of the decay curve. Substituting the approximated formulae based on the experimental data for the decay curves for the parameters of k and ε into the formula for v_t we obtain the expression

$$v_t = \frac{3}{2} c_\mu \frac{MU}{C}.$$

Let us designate the constant C for the single-phase flow as C_0 and the corresponding one for the two-phase flow as C_s. From the Eqs. (1)–(4) we can conclude for our study that $C_s > C_0$. Hence, the ratio of the turbulent viscosities is as follows

$$\frac{v_{ts}}{v_{t0}} = \frac{3 c_\mu MU}{2 C_s \frac{3}{2} c_\mu MU / C_0} = \frac{C_0}{C_s} < 1. \tag{5}$$

This means that the turbulent viscosity for the two-phase flow v_{ts} is smaller than the corresponding one for the single-phase flow, namely v_{t0}.

On the other hand, according to the hypothesis of Heisenberg (Hinze, 1975) the turbulent viscosity of eddies related to the wave number **k** is as follows

$$v_t = \int_k^\infty \sqrt{\frac{E(k,t)}{k^3}}\, \mathrm{d}k,$$

i.e., the turbulent viscosity is determined by the high-frequency sub-range of spectrum. Therefore, the reduction of the turbulent viscosity in the two-phase flow must be due to the decrease of the energy spectrum density in the high-frequency sub-range, that was observed in the present experiments.

7. Conclusion

The presented experimental studies concentrated on the influence of solid particles on the turbulence modulation in case of dilute two-phase vertical flow. The coarse particles considered, attenuated the grid-generated turbulence resulting in an increase of the dissipation rate of turbulence and a decrease of the turbulent energy in the sub-range of the energy-containing eddies. Apparently, one can expect the generation of turbulence by coarse particles with increasing of their mass loading. In this connection it is expediently to continue the

experimental investigations with higher particle mass loading where the influence of particles on the turbulence decay of the carrier flow would be examined. Moreover, the influence of the Stokes number (mainly influenced by the particle size and the material density) on the turbulence modulation of the carrier flow is of major interest as well.

Acknowledgements

Financial supports by the Volkswagen Foundation (project no. 1/71 211) and the Estonian Science Foundation (grant no. 1471) are gratefully acknowledged.

References

Gore, R.A., Crowe, C.T., 1989. Effect of particle size on modulating turbulent intensity. Brief communication. Int. J. Multiphase Flow 15 (2), 279–285.

Gore, R.A., Crowe, C.T., 1991. Modulation of turbulence by a dispersed phase. J. Fluids Engrg. 113 (6), 304–307.

Gorlin, S.M., 1970. Experimental air-mechanics. p. 423 (in Russian).

Crowe, C.T., Troutt, T.R., Chung, J.N., 1996. Numerical models for two-phase turbulent flows. Annu. Rev. Fluid Mech. 28, 11–43.

Durst, F., 1982. Review-combined measurements of particle velocities, size distributions, and concentrations. Transactions of the ASME. J. Fluids Engrg. 104, 284–296.

Durst, F., 1983. Development of measuring techniques for particle velocity, particle size and particle concentration. Wasserwirtschaft 11 (73), 469–475.

Elghobashi, S., 1991. Particle-laden turbulent flows: direct simulation and closure models. In: Oliemans, R.V.A. (Ed.), Computational fluid Dynamics for the Petrochemical Process Industry, vol. 48, Applied Scientific Research. Kluwer Academic Publishers, Dordrecht, pp. 301–314.

Frishman, F.A., Rozenstein, A.Z., Shcheglov, I.N., 1987. Experimental set-up for determination of parameters of two-phase "gas–solid particles" turbulent flows. Physical methods for investigations of the transparent heterogeneous flows. The All-Union Workshop, Moscow, pp. 41-45 (in Russian).

Hetsroni, G., 1989. Particles–turbulence interaction. Int. J. Multiphase Flow 15 (5), 735–746.

Hinze, J.O., 1975. Turbulence, second ed. McGraw-Hill, New York, p. 790.

Kartushinsky, A.I., Rozenstein, A.Z., Shcheglov, I.N., 1987. Quantitative assessment of "optical signals" in LDA systems in conformity with the problem of diagnostic of two-phase flows. Physical methods for investigations of the transpatent heterogeneous flows. The All-Union Workshop, Moscow, pp. 29–33 (in Russian).

Kenning, V.M., Crowe, C.T., 1997. On the effect of particles on carrier phase turbulence in gas-particle flows. Brief communication. Int. J. Multiphase Flow 23 (2), 403–408.

Kulick, J.D., Fessler, J.R., Eaton, J.K., 1993. On the interactions between particles and turbulence in a fully-developed channel flow in air. Report No. MD-66, Thermosciences Division, Department of Mechanical Engineering, Stanford University, Stanford, California, USA, p. 195.

Kulick, J.D., Fessler, J., Eaton, J.K., 1994. Particle response and turbulence modification in fully developed channel flow. J. Fluid Mech. 277, 109–134.

Laats, M.K., Frishman, F.A., 1970. Assumptions used for the calculation of the two-phase turbulent jet. Izv. Acad. Nauk SSSR, Mekh. Zhidk, Gaza 2, 186–191.

Lance, M., Bataille, J., 1991. Turbulence in the liquid phase of a uniform bubbly air–water flow. J. Fluid Mech. 222, 95–118.

Marple Jr., S.L. (Ed.), 1987. Digital Spectral Analysis with Applications. Prentice-Hall, Englewood Cliffs, NJ, pp. 584.

Schreck, S., Kleis, S.J., 1993. Modification of grid-generated turbulence by solid particles. J. Fluid Mech. 249, 665–688.

Snyder, W.H., Lumley, J.L., 1971. Some measurements of particle velocity auto-correlation functions in a turbulent flow. J. Fluid Mech. 1 (1), 41–71.

Van de Hulst, H.C., 1957. Light Scattering by Small Particles. Wiley New York, Chapman & Hall, London, p. 536.